Supporting information for

Rational Cyano Functionalization of Copper Phenylacetylide Paves the Way for Superior Photogenerated Electron Transport Capability and Diclofenac Degradation

Lingrong Chen[a], Yishun Wang[a], Fengyuan Zhang[b], Yanfang Wang[b], Yunshuang He[b], Hongda Zhan[a], Xiaoyu Zhang[a], Ping Chen[a,], Zili Lin [a,*], Wenying Lv[a,*], Guoguang Liu[a]*

[a] *Guangdong Key Laboratory of Environmental Catalysis and Health Risk Control, School of Environmental Science and Engineering, Institute of Environmental Health and Pollution Control, Guangdong University of Technology, Guangzhou 510006, China*

[b] *Guangzhou Wang Lao Ji Great Health Industry Co., Ltd., Guangzhou 510623, China*

* **Corresponding Author**: Ping Chen; Zili Lin; Wenying Lv

E-mail: gdutchp@163.com (P. Chen); zlin9811@163.com (Z. Lin); lvwy612@163.com (W. Lv)

Tel: +86-15018448140 (P. Chen); +86-18138116133 (Z. Lin); +86-13538982812 (W. Lv)

Catalogue

1 Texts

Text S1. Materials

Diclofenac (DCF, AR) and 4-hydroxy-2,2,6,6-tetramethylpiperidinyloxy (TEMPOL, AR) were purchased from the Aladdin Industrial Company, China. Sodium oxalate ($Na_2C_2O_4$), tert-Butyl alcohol (TBA, AR), HCl (AR), and NaOH (AR) were obtained from the Chemical Reagent Factory, China. Ultrapure water (18.25 MΩ·cm) supplied by a water purification system (NC-BF10, NICO, China) was utilized for all experiments.

Text S2. Characterizations

The morphologies of PhC_2Cu and Cy-PhC_2Cu were observed by scanning electron microscopy (SEM, SU8200, Hitachi, Japan). The morphology and composition of Cy-PhC_2Cu composites were observed by transmission electron microscopy (TEM, Talos F200S, Fisher, USA). An X-ray diffractometer (XRD, X 'PERT PRO MPD, Netherlands) was used to characterize the crystalline structure of the prepared materials. Fourier transform infrared spectroscopy (FT-IR, Nicolet 6700, Thermo Fisher, USA) was used to characterize the characteristic chemical bonds of the prepared materials. The specific surface area of the material was determined using an automatic specific surface area and porosity analyzer (BET, Micromeritics Tristar 3000, USA). The chemical elements of the prepared materials were analyzed by X-ray photoelectron spectroscopy (XPS, Thermo Fisher, USA). The absorption properties of the photocatalytic materials for visible light were tested with UV-3600 Plus, SHIMADZU, Japan. Photoluminescence (PL) spectra were measured using a fluorescence spectrophotometer (F-4600, Hitachi, Japan) with an excitation wavelength of 378 nm. The intermediate products in the degradation process of diclofenac are detected by high performance liquid chromatography-mass spectrometry (HPLC-MS, Q Exactive, China). The concentration of residual DCF in the samples was determined by liquid chromatograph (HPLC, LC16, SHIMADZU, Japan) with the detection wavelength at 278 nm, column temperature at 35 °C, and sample volume at 20 μL. The main active species in the system were determined by adding quencher, and further verified by electron paramagnetic resonance test (EPR, JES FA 200, JEOL, Japan). All characterization methods are based on CyP-1.0.

Text S3. Photoelectrochemical measurements

The photoelectrochemical properties of the photocatalysts were investigated using a CEL-NF2000 light power meter (Beijing Zhongjiao Jinyuan Technology Co.; China) electrochemical workstation. A Pt wire electrode served as the counter electrode, and an Ag/AgCl electrode (NHE) acted as the reference electrode. 0.1 M Na_2SO_4 aqueous solution was used as the electrolyte. For the preparation of the working electrode, 25 mg of the samples were dispersed in 0.4 mL of ethanol and mixed with 60 uL of Nafion 117. The resulting suspension was ultrasonically treated and drop-coated onto ITO glass (1 cm × 1 cm).

In the light response current curve (i-t) experiment, the open circuit voltage test was conducted first, selecting an appropriate bias voltage for dark current measurement. The light baffle was switched every 30 s during this period to alternately test light and dark currents. The current reading on the electrochemical workstation was paused during baffle switching and resumed after the material's current stabilized.

In the electrochemical impedance spectroscopy (EIS) experiment, the open circuit voltage test was performed initially, and the curve values were measured with a frequency ranging from 105 Hz to 0.01 Hz.

Bragg equation

$$2d\sin\theta=n\lambda \tag{S1}$$

Where d is the interplanar spacing of the crystal, θ is the angle between the incident X-ray and the crystal plane, n is the diffraction order, and λ is the wavelength of the X-ray.

Tauc formula

$$\alpha h\nu=A(h\nu-E_g)^{1/2} \tag{S2}$$

Where α is the absorption coefficient, A is the constant, hν is the photon energy, h is the Planck constant, ν is the incident photon frequency, Eg is the semiconductor bandgap width (bandgap).

$$E_{CB} = E_{VB} - E_g \tag{S3}$$

Where, E_{CB} is a semiconductor conduction band (eV); E_{VB} is semiconductor price band (eV); Eg is Band gap (eV).

Text S4. Photocatalytic experiment

The filtered sample was detected by High-Performance Liquid Chromatography (HPLC) system (Shimadzu HPLC-20A, Japan). The calculation method of DCF removal rate R is shown in Eq. (S4). In order to further study the reaction kinetics characteristics of Cy-PhC_2Cu system to DCF degradation, linear fitting was performed according to the pseudo-first-order reaction kinetics model. The calculation formula for photocatalytic rate is shown in Eq. (S5).

$$\mathrm{R} = \frac{C_0 - C_t}{C_0} \times 100\% \tag{S4}$$

$$\ln\left(\frac{C_t}{C_0}\right) = -K_{obs}t \tag{S5}$$

Where R is the removal rate of DCF, C_0 is the initial concentration of DCF (10 mg·L^{-1}), C_t is the concentration of DCF at time t, K_{obs} is the pseudo-first-order kinetic constant (min^{-1}), and t is the reaction time (min).

Text S5. Quenching experiment

To identify the main reactive species (ROS), radical quenching experiments were conducted to quench the corresponding ROS through the addition of different scavengers during the photocatalytic process. The scavengers used included 0.1 g of 4-hydroxy-2,2,6,6-tetramethylpiperidinyloxy (TEMPOL), 0.0335 g of sodium oxalate ($Na_2C_2O_4$), 0.1 mL of furfuryl alcohol (FFA) and 0.2 mL tert-Butyl alcohol (TBA) for superoxide ($^{\cdot}O_2^-$), holes (h^+), singlet oxygen ($^1O_2$) and hydroxyl (·OH), respectively.

$$R_{\cdot O_2^-} = \frac{K_{\cdot O_2^-}}{K_{\mathrm{DCF}}} \approx 1 - \frac{K_{\mathrm{TEMPOL}}}{K_{\mathrm{DCF}}} \tag{S6}$$

$$R_{h^+} = \frac{K_{h^+}}{K_{\mathrm{DCF}}} \approx 1 - \frac{K_{Na_2C_2O_4}}{K_{\mathrm{DCF}}} \tag{S7}$$

$$R_{\cdot OH} = \frac{K_{^1O_2}}{K_{\mathrm{DCF}}} \approx 1 - \frac{K_{\mathrm{FFA}}}{K_{\mathrm{DCF}}} \tag{S8}$$

$$R_{^1O_2} = \frac{K_{\cdot OH}}{K_{\mathrm{DCF}}} \approx 1 - \frac{K_{\mathrm{TBA}}}{K_{\mathrm{DCF}}} \tag{S9}$$

In the Eqs. (S6-9), R (%) signifies the contribution of reactive species to the photocatalytic degradation of DCF, while K (min^{-1}) denotes the reaction rate constant.

Text S6. Synthesis of PhC_2Cu

The PhC_2Cu was synthesized using a solvothermal method adopted from the literature. The samples were synthesized through combining $CuCl_2 \cdot 2H_2O$ (0.365 g), CH_3OH (50 mL), triethylamine (Et_3N, 1.12 ml), and phenyl acetylene (0.44 ml) in a beaker, then heating to 70 °C for about 25 min. The reaction was stopped immediately once the flocculant turned light yellow. Finally, the PhC_2Cu was centrifuged and rinsed, and then collected by drying at 60 °C overnight.

2 Tables

Table S1. HPLC parameters of NSAID.

NSAID	Mobile phase composition	Column Temperature	Detection wavelength	Chromatographic Column
Diclofenac	Methanol: 0.2% formic acid 80:20 (v:v)	35 °C	276 nm	Agilent Eclipse XDB-C18 5 um (4.6×150 mm)

Table S2. BET specific surface area and total pore volume of PhC_2Cu and Cy-PhC_2Cu.

Adsorbents	Surface Area ($m^2 \times g^{-1}$)	Pore Volume ($cm^3 \times g^{-1}$)	Pore Size (nm)
PhC_2Cu	37.6799	0.2566	27.2416
Cy-PhC_2Cu	36.5930	0.1910	20.8721

Table S3. Actual water sampling information.

Water sample	Sampling location	Sampling date
Lake water	Haizhu Lake, Guangzhou. Guangdong Province, China.	May 3, 2024, 15: 20 p.m.
Tap-water	Guangdong University of Technology, Guangzhou, Guangdong Province, China.	May 12, 2024, 10: 00 a.m.
River water	Raoping, Chaozhou, Guangdong Province, China	June 14, 2024, 15: 30 p.m.
Seawater	Raoping, Chaozhou, Guangdong Province, China	June 16, 2024, 16: 00 p.m.

Table S4. Comparison with other materials for the photocatalytic degradation.

Photocatalyst	Dosage	Initial Concentration	Light Source	K_{obs} (min^{-1})	Photocatalytic Performance	Ref.
$Bi_2O_{2.33}/Bi_4O_5I_2$	167mg/L	20 mg/L	λ > 420 nm (300 W)	0.0275	97.58 % (200 min)	[1]
Biomass C/Bi_2WO_6	1000 mg/L	8 mg/L	λ < 420 nm (500 W)	/	96.19 % (120 min)	[2]
In-CE_2（$MoO_4)_3$/g-C_3N_4	10 mg/L	10 mg/L	λ > 420 nm (150 W)	/	87.0 % (105 min)	[3]
g-C_3N_4-PVDF	500 mg/L	250 μg/L	λ < 405 nm (300 W)	/	72.0 % (24 h)	[4]
La/TiO_2	500 mg/L	50 ppm	λ > 400 nm (12 W)	0.0016	/ (240 min)	[5]
N/TiO_2/rGO	250 mg/L	10 mg/L	λ > 420 nm (70 W)	0.0276	91.08 % (120 min)	[6]
Ag/ g-C_3N_4	100 mg/L	100 mg/L	λ > 400 nm (300 W)	0.0429	100 % (120 min)	[7]
TiO_2/ZrO_2	250 mg/L	10 mg/L	λ = 8 nm (210 W)	/	92.41 % (210 min)	[8]
Cy-PhC_2Cu	**200 mg/L**	**10 mg/L**	**9 W 6.1 mW/cm^2 LED (λ = 455 nm)**	**0.0339**	**96.76% (100 min)**	**This work**

Table S5. Transformation intermediates for Cy-PhC_2Cu degradation of DCF.

Product	Molecular Formula	Mw	MS^2/[M+H]-	Probable Structure
P1	$C_{14}H_{11}Cl_2NO_2$	296	296.0237	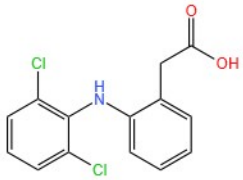
P2	$C_{14}H_{11}Cl_2NO_3$	312	312.0184	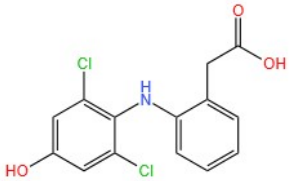
P3	$C_6H_5Cl_2NO$	178	177.9562	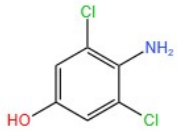
P4	$C_{14}H_{12}ClNO_3$	294	294.0557	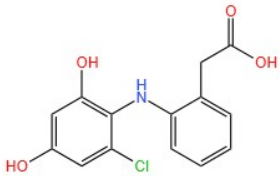
P5	$C_{14}H_{12}ClNO_5$	310	310.0028	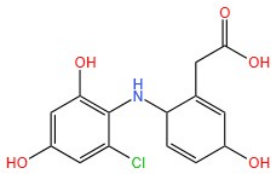
P6	$C_{14}H_{10}ClNO_5$	308	308.0886	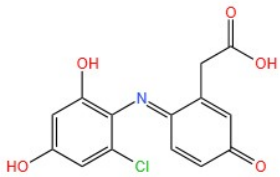
P7	$C_{13}H_{11}Cl_2N$	252	252.0153	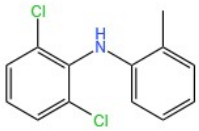
P8	$C_{13}H_{10}ClN$	216	216.0386	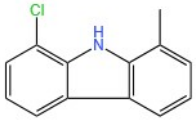

P9	C_7H_9N	108	108.2989	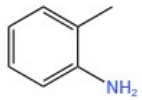
P10	$C_{14}H_{11}Cl_2NO_3$	312	312.0185	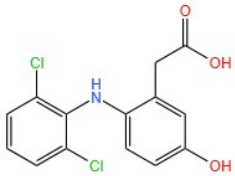
P11	$C_{14}H_9Cl_2NO_3$	310	310.0028	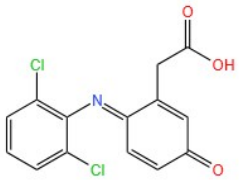
P12	$C_{13}H_9Cl_2NO$	266	266.1724	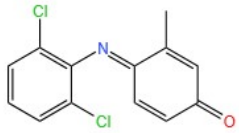
P13	$C_{13}H_9Cl_2NO_2$	282	282.2037	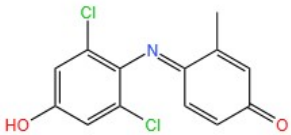
P14	$C_6H_5Cl_2N$	162	161.9814	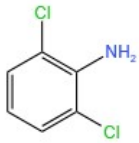

Table S6. Pollutant degradation kinetics.

degradation kinetics	zero-order		first-order		second-order	
	k (mg·L^{-1}·min^{-1})	R^2	k (min^{-1})	R^2	k (L·mg^{-1}·min^{-1})	R^2
PhC_2Cu	0.03180	0.96014	0.00565	0.98238	0.00109	0.99059
CyP-0.5	0.03429	0.98705	0.00635	0.95914	0.00114	0.88677
CyP-1.0	0.07719	0.99075	0.03385	0.99451	0.00665	0.33341
CyP-1.5	0.05221	0.99302	0.01015	0.98888	0.00119	0.98500

Table S7. Copper dissolution rate.

Sample	Copper content in the sample (mg/L)
PhC_2Cu	2.85
Cy-PhC_2Cu	5.20

3 Figures

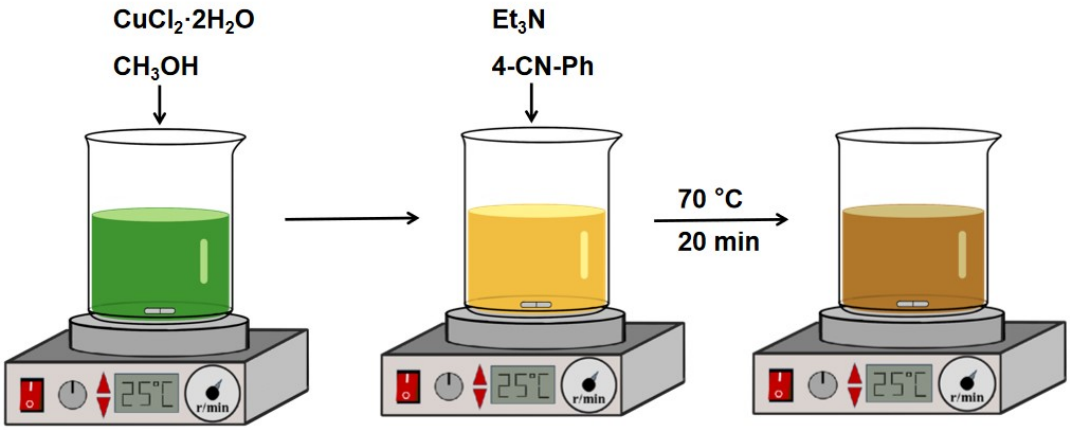

Fig. S1 Synthesis of Cy-PhC_2Cu

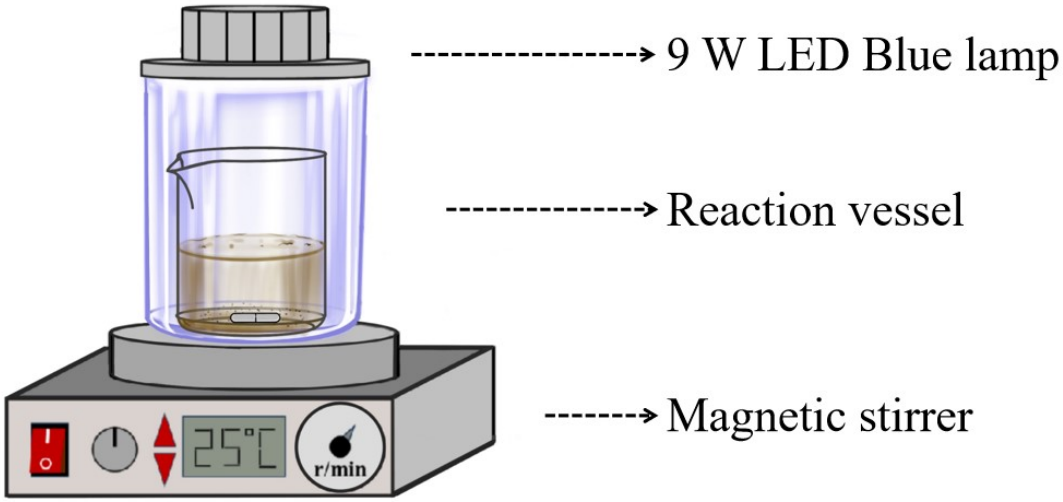

Fig. S2 Photocatalytic reaction device.

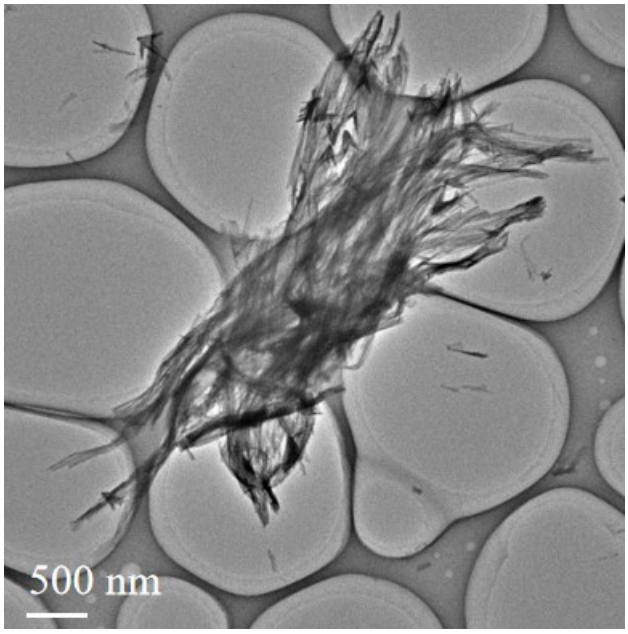

Fig. S3 TEM images of Cy-PhC_2Cu.

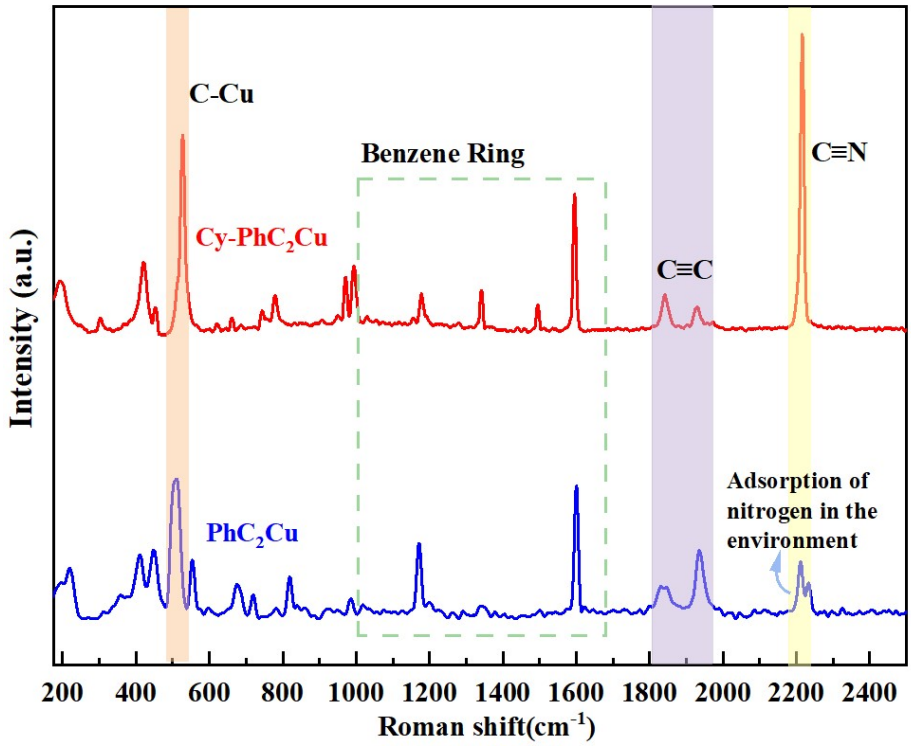

Fig. S4 Raman spectrum of PhC_2Cu and Cy-PhC_2Cu.

In Fig. S4, the Raman spectra of PhC_2Cu at approximately 1018, 1170, and 1599 cm^{-1} are characteristic lines of the benzene ring. The Raman bands at 1834 and 1938 cm^{-1} may be attributed to Fermi resonance and second-order transitions enhanced by v (C≡C).[9] The Raman band at 509 cm^{-1} may be attributed to the vibration generated by the coordination interaction between copper and phenylacetylene. It is worth noting that the Raman band of PhC_2Cu at 2214cm^{-1} can be attributed to the adsorbed nitrogen-containing compound, which is consistent with the research of Zhao et al.,[10] and due to the introduction of the cyano group, Cy-PhC_2Cu exhibits stronger Raman vibrations at the corresponding location.

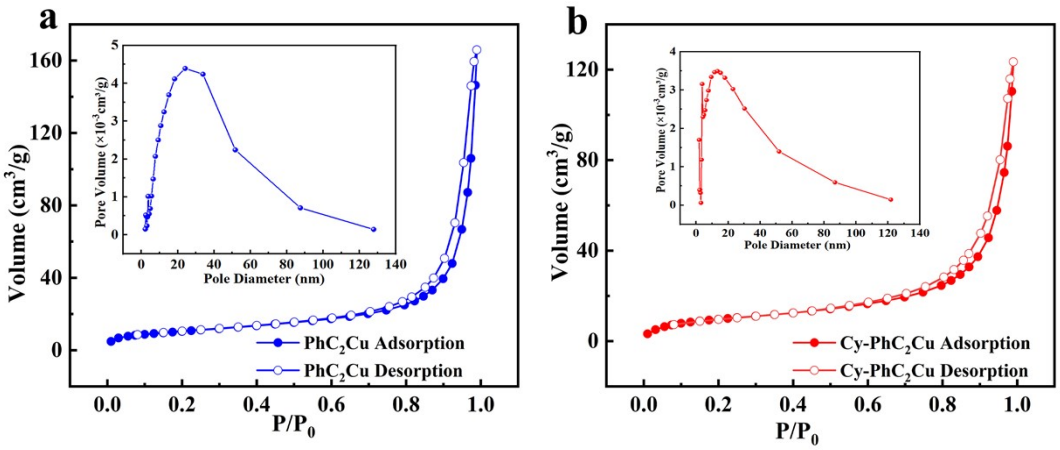

Fig. S5 N_2 adsorption-desorption isotherms (inset shows BJH pore-size distribution) of PhC_2Cu (a) and Cy-PhC_2Cu (b).

The surface properties of the photocatalysts were characterized by N_2 adsorption-desorption analysis (Fig. S5). Both synthesized catalysts exhibited type IV isotherms, confirming their mesoporous structures. According to Table S2, due to the three-dimensional effect of -CN occupying the pore size, the introduction of cyano did not significantly change the specific surface area of the material, indicating that its adsorption capacity may decrease.

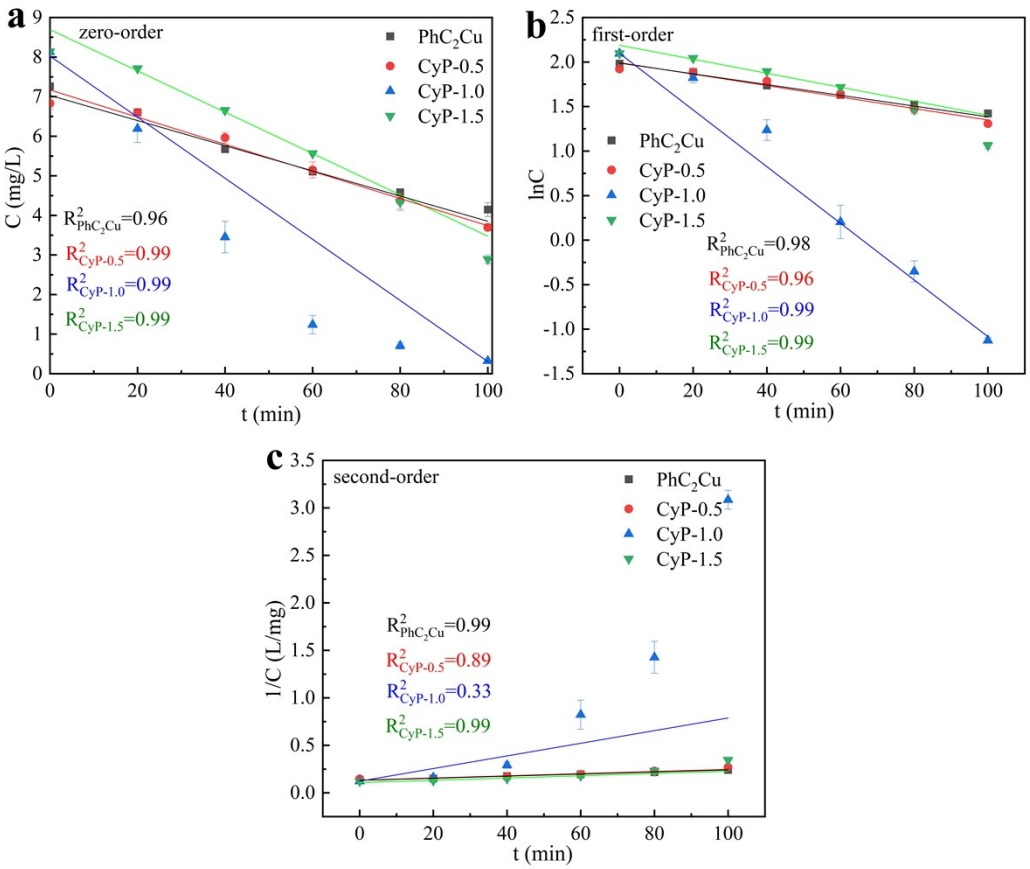

Fig. S6 Pollutant degradation kinetics (zero-order, first-order, and second-order).

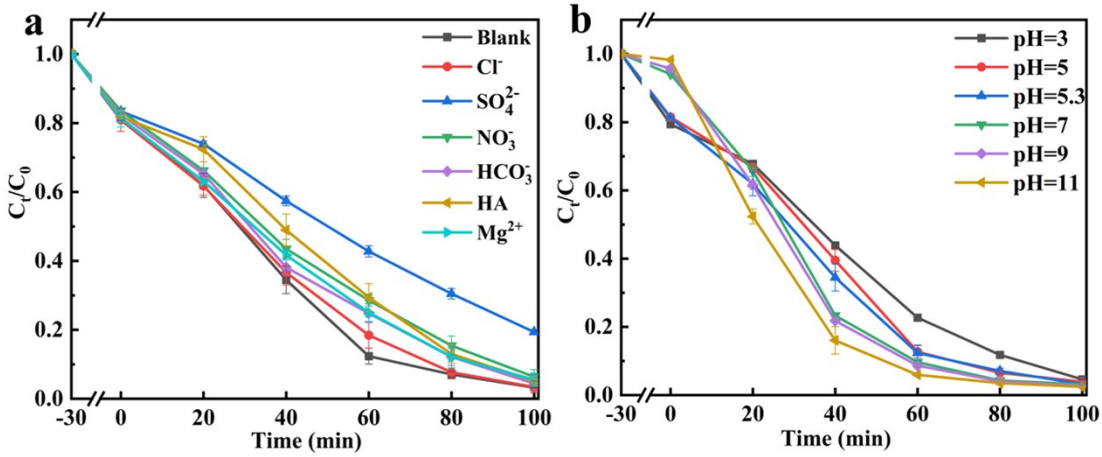

Fig. S7 Photocatalytic degradation of DCF in different ions (a). Photocatalytic degradation of DCF in different pH (b).

In Fig. S7a, photocatalytic degradation experiments of DCF were carried out under blank control condition, Cl^-, SO_4^{2-}, NO_3^-, HCO_3^-, HA and Mg^{2+}, respectively. The degradation efficiencies of DCF were 96.76%, 96.61%, 80.63%, 93.66%, 95.58%, 94.82% and 94.49%, respectively. In addition, testing the degradation degree of DCF at pH 3, 5, 5.3 (blank control), 7, 9 and 11, and the degradation efficiencies were 95.41%, 96.06%, 96.76%, 96.87%, 97.26% and 97.55%, respectively (Fig. S7b).

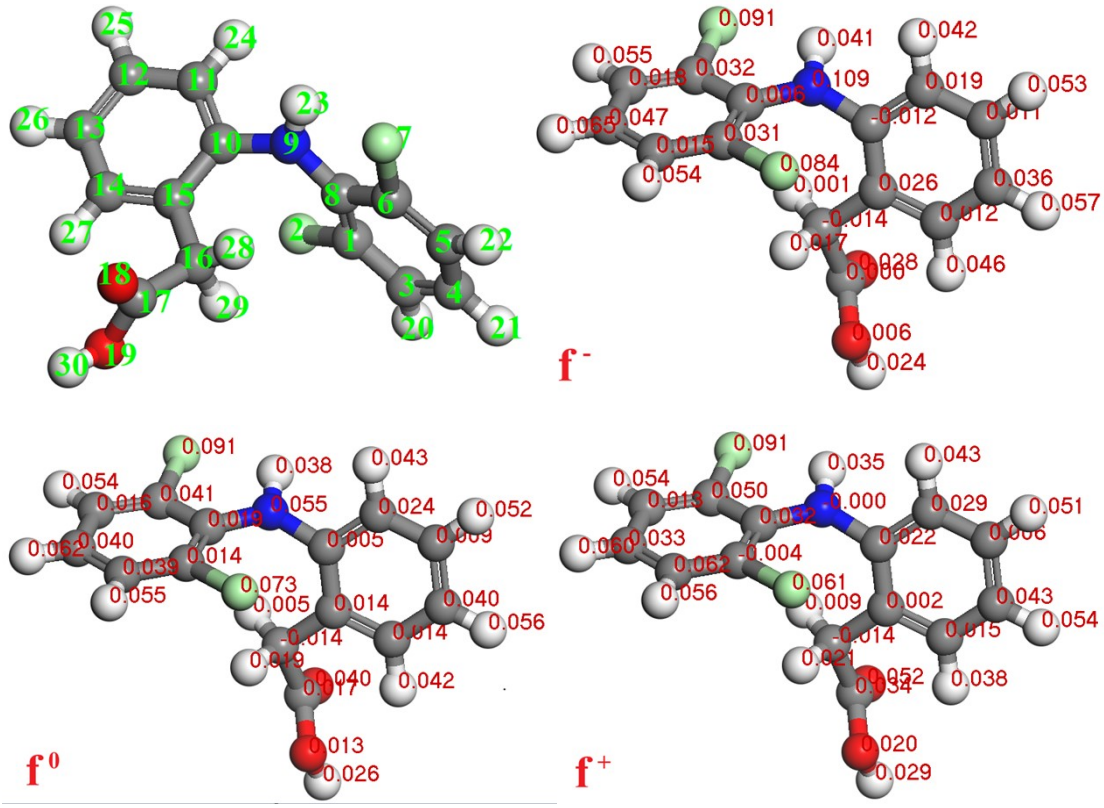

Fig. S8 Calculated Fukui-index of DCF.

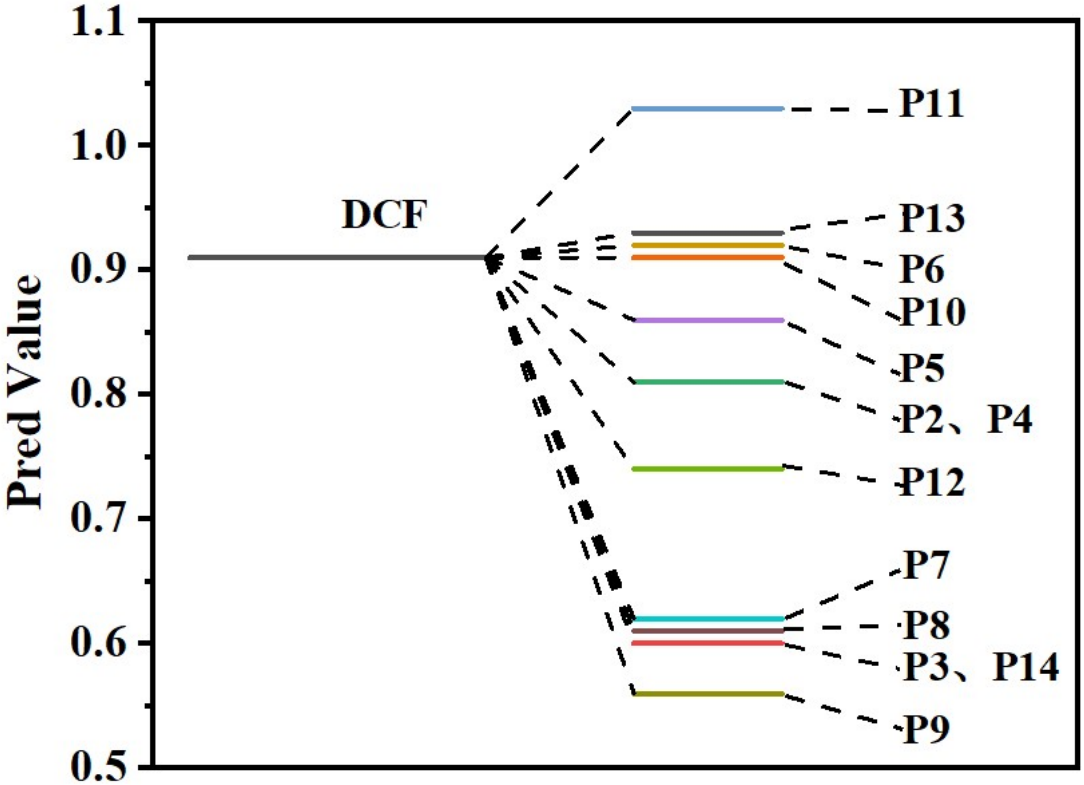

Fig. S9 The developmental toxicity of DCF intermediates.

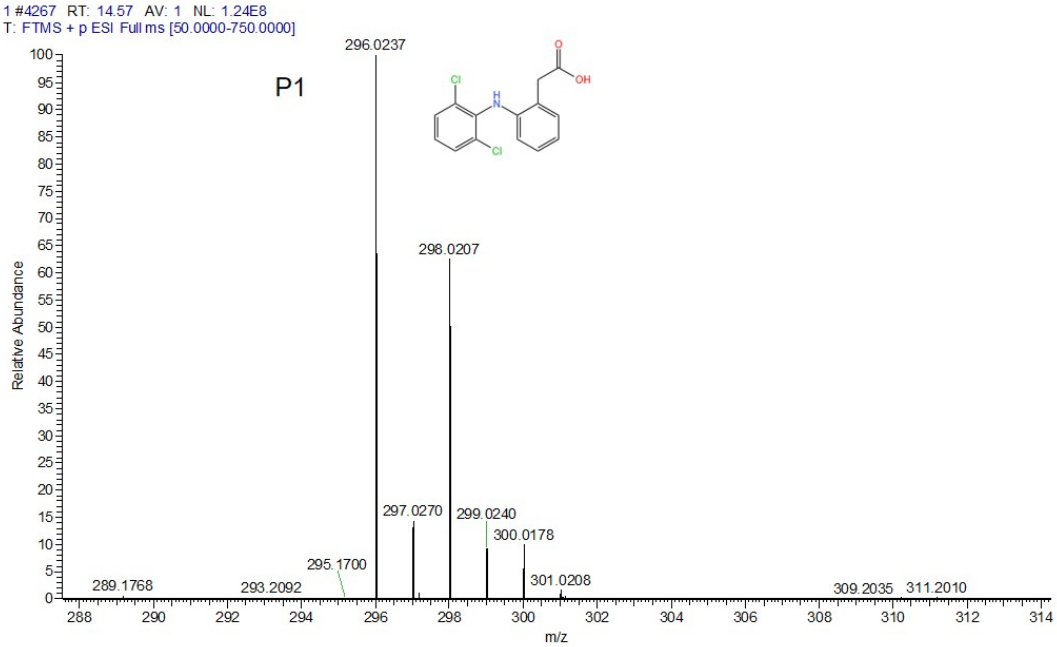
1 #4267 RT: 14.57 AV: 1 NL: 1.24E8
T: FTMS + p ESI Full ms [50.0000-750.0000]
P1
296.0237
298.0207
297.0270
299.0240
300.0178
295.1700
301.0208
289.1768
293.2092
309.2035
311.2010
Relative Abundance
m/z

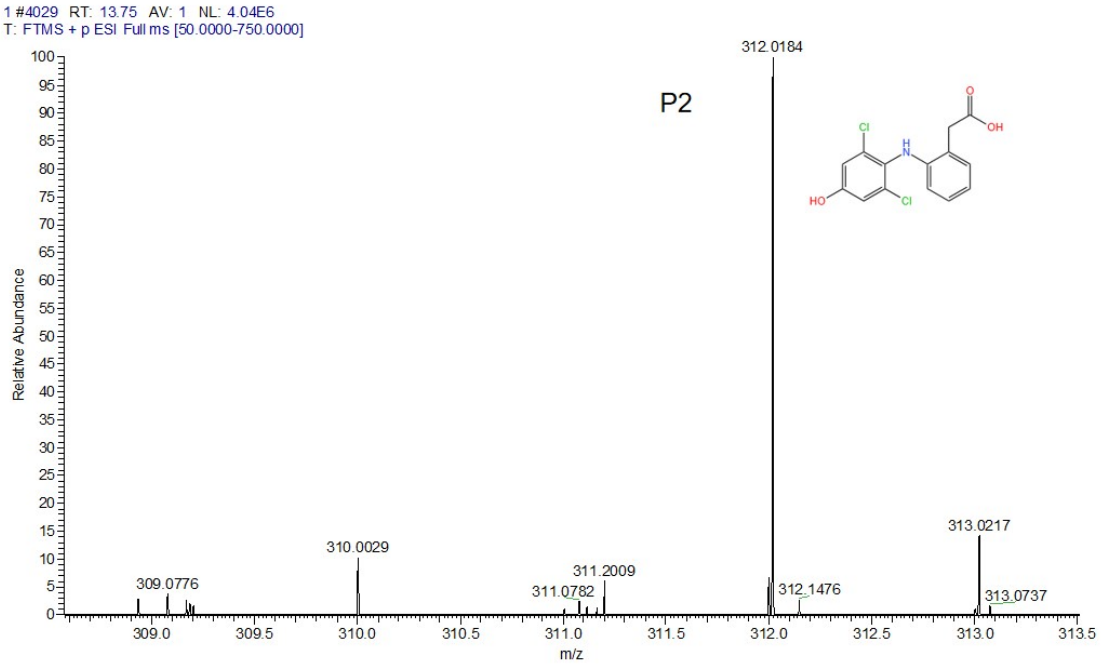
1 #4029 RT: 13.75 AV: 1 NL: 4.04E6
T: FTMS + p ESI Full ms [50.0000-750.0000]
P2
312.0184
313.0217
310.0029
311.2009
309.0776
311.0782
312.1476
313.0737
Relative Abundance
m/z

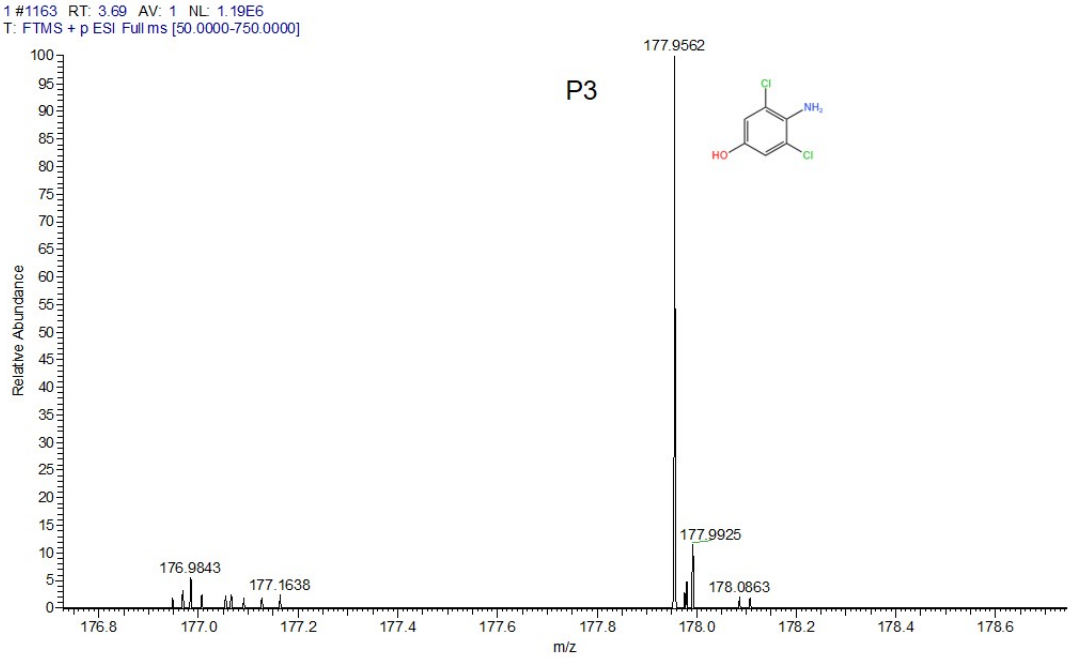
1 #1163 RT: 3.69 AV: 1 NL: 1.19E6
T: FTMS + p ESI Full ms [50.0000-750.0000]
P3
177.9562
177.9925
176.9843
177.1638
178.0863
Relative Abundance
m/z

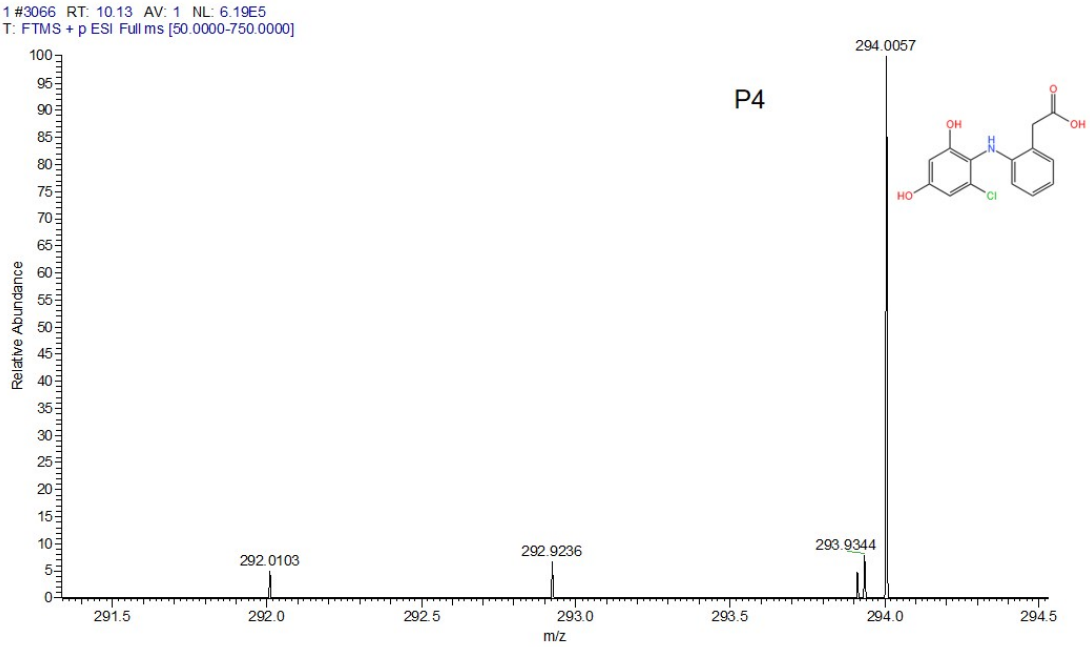
1 #3066 RT: 10.13 AV: 1 NL: 6.19E5
T: FTMS + p ESI Full ms [50.0000-750.0000]
P4
294.0057
292.0103
292.9236
293.9344
Relative Abundance
m/z

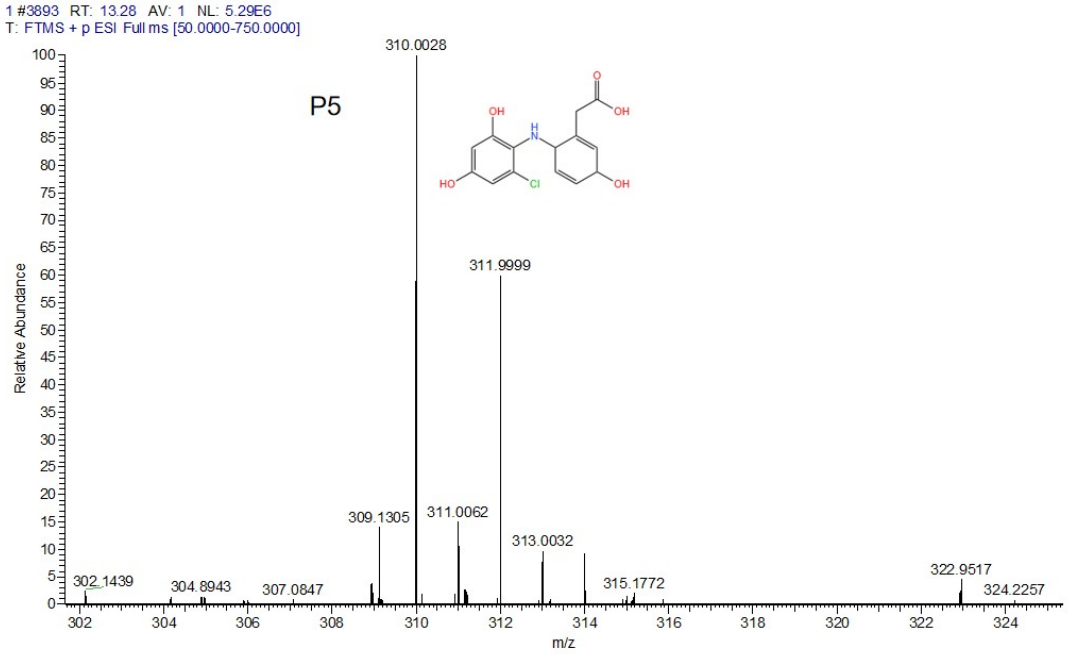
1 #3893 RT: 13.28 AV: 1 NL: 5.29E6
T: FTMS + p ESI Full ms [50.0000-750.0000]
P5
310.0028
311.9999
309.1305
311.0062
313.0032
302.1439
304.8943
307.0847
315.1772
322.9517
324.2257
Relative Abundance
m/z

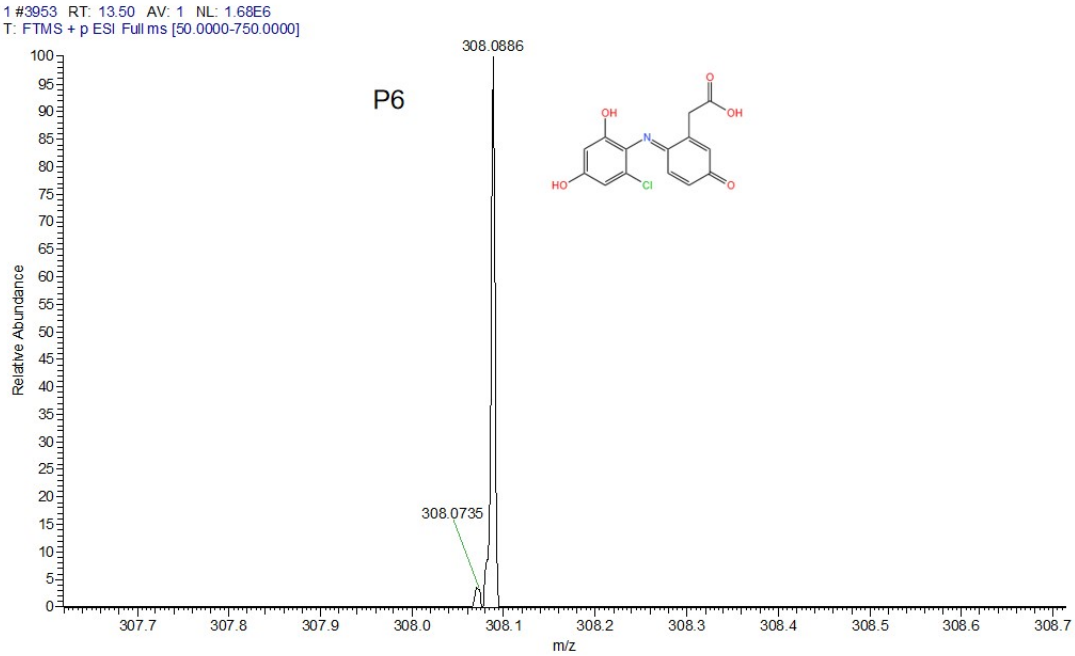
1 #3953 RT: 13.50 AV: 1 NL: 1.68E6
T: FTMS + p ESI Full ms [50.0000-750.0000]
P6
308.0886
308.0735
Relative Abundance
m/z

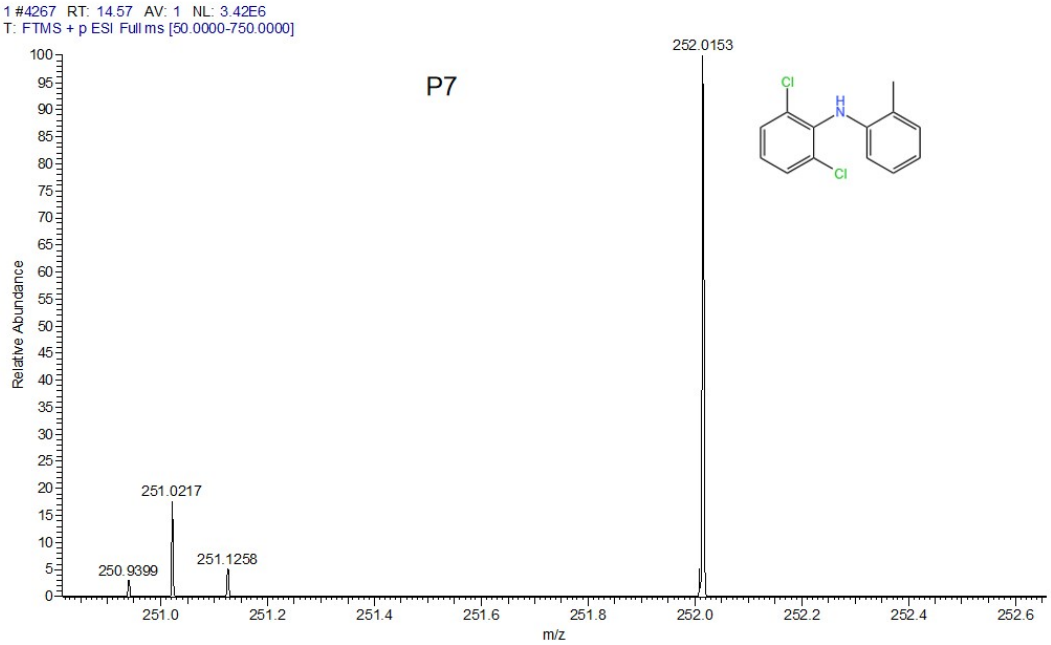
1 #4267 RT: 14.57 AV: 1 NL: 3.42E6
T: FTMS + p ESI Full ms [50.0000-750.0000]
P7
252.0153
251.0217
251.1258
250.9399
Relative Abundance
m/z

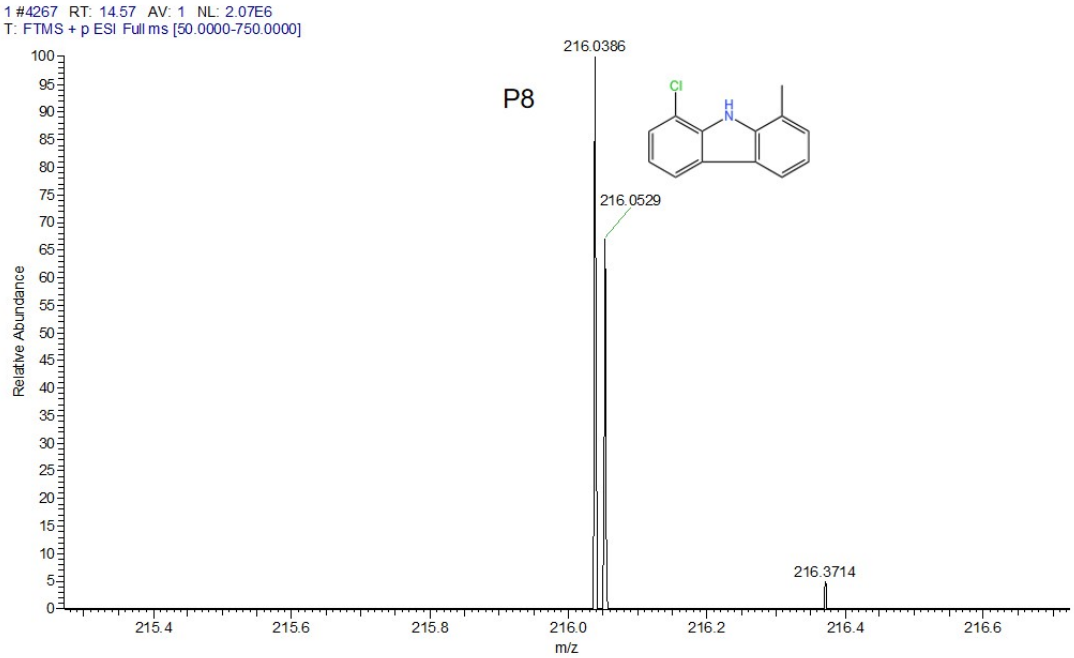
1 #4267 RT: 14.57 AV: 1 NL: 2.07E6
T: FTMS + p ESI Full ms [50.0000-750.0000]
P8
216.0386
216.0529
216.3714
Relative Abundance
m/z

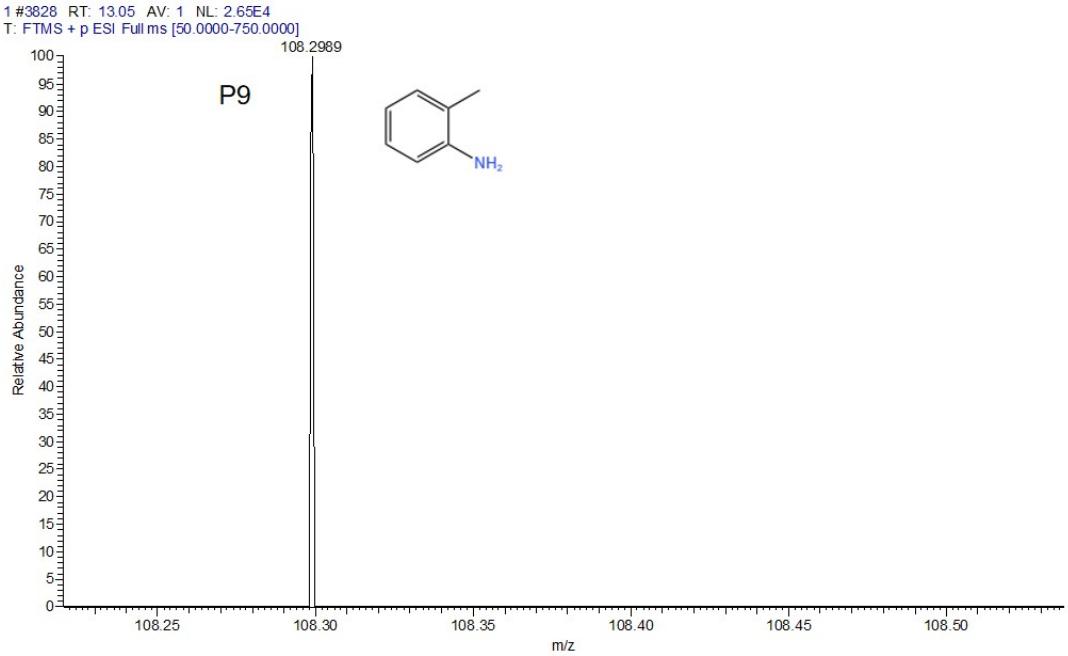
1 #3828 RT: 13.05 AV: 1 NL: 2.65E4
T: FTMS + p ESI Full ms [50.0000-750.0000]
108.2989
P9
NH2
Relative Abundance
m/z

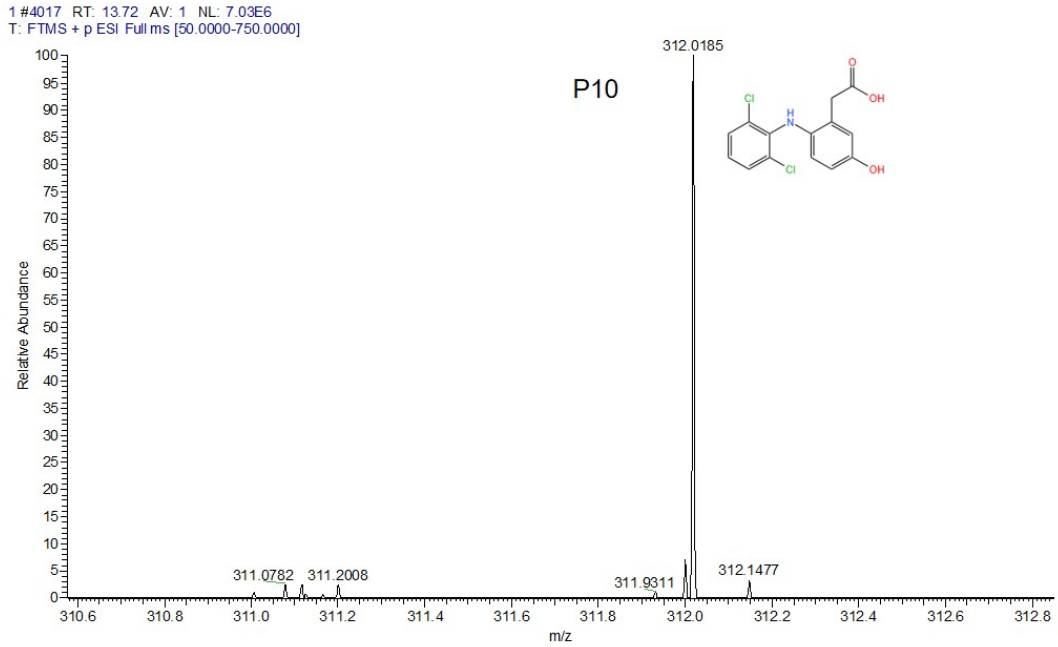
1 #4017 RT: 13.72 AV: 1 NL: 7.03E6
T: FTMS + p ESI Full ms [50.0000-750.0000]
312.0185
P10
Cl
H
N
O
OH
Cl
OH
311.0782
311.2008
311.9311
312.1477
Relative Abundance
m/z

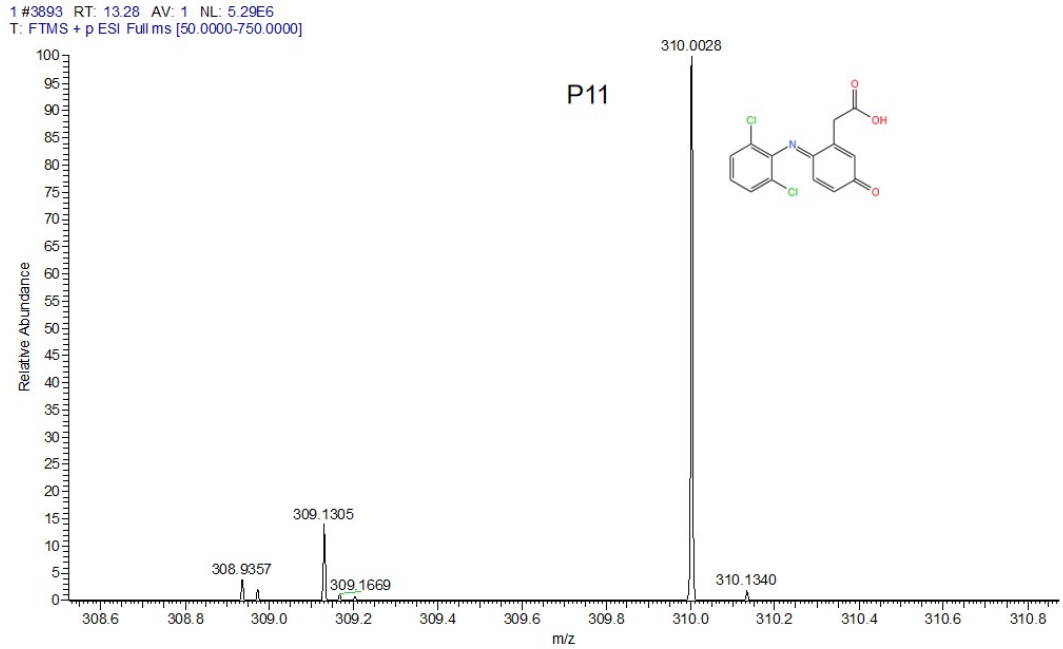
1 #3893 RT: 13.28 AV: 1 NL: 5.29E6
T: FTMS + p ESI Full ms [50.0000-750.0000]
P11
310.0028
309.1305
308.9357
309.1669
310.1340
Relative Abundance
m/z

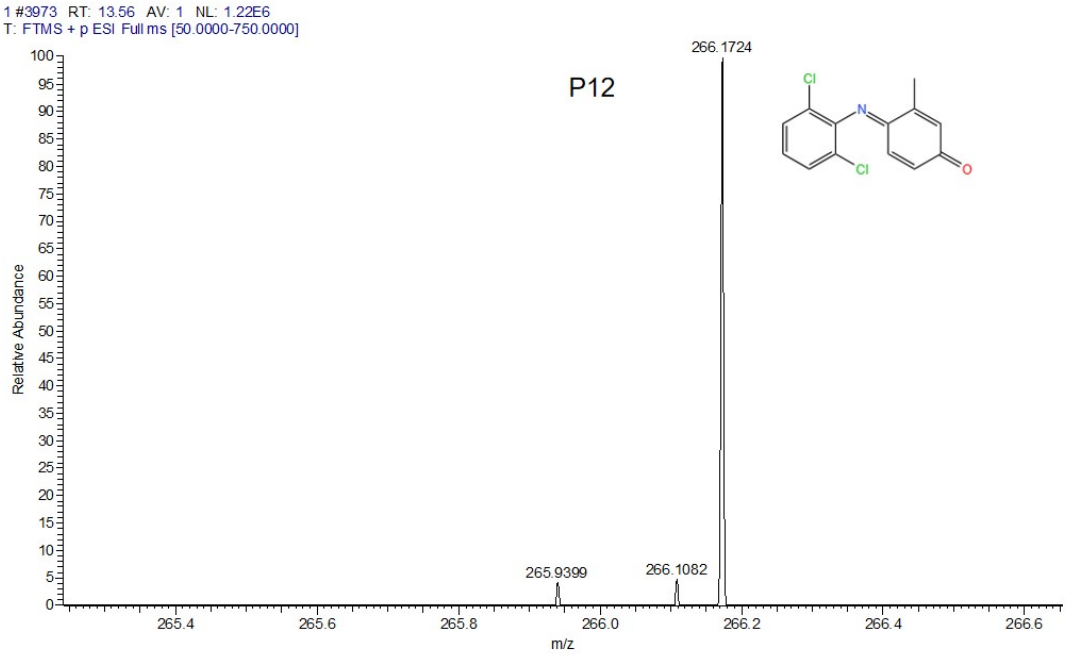
1 #3973 RT: 13.56 AV: 1 NL: 1.22E6
T: FTMS + p ESI Full ms [50.0000-750.0000]
P12
266.1724
265.9399
266.1082
Relative Abundance
m/z

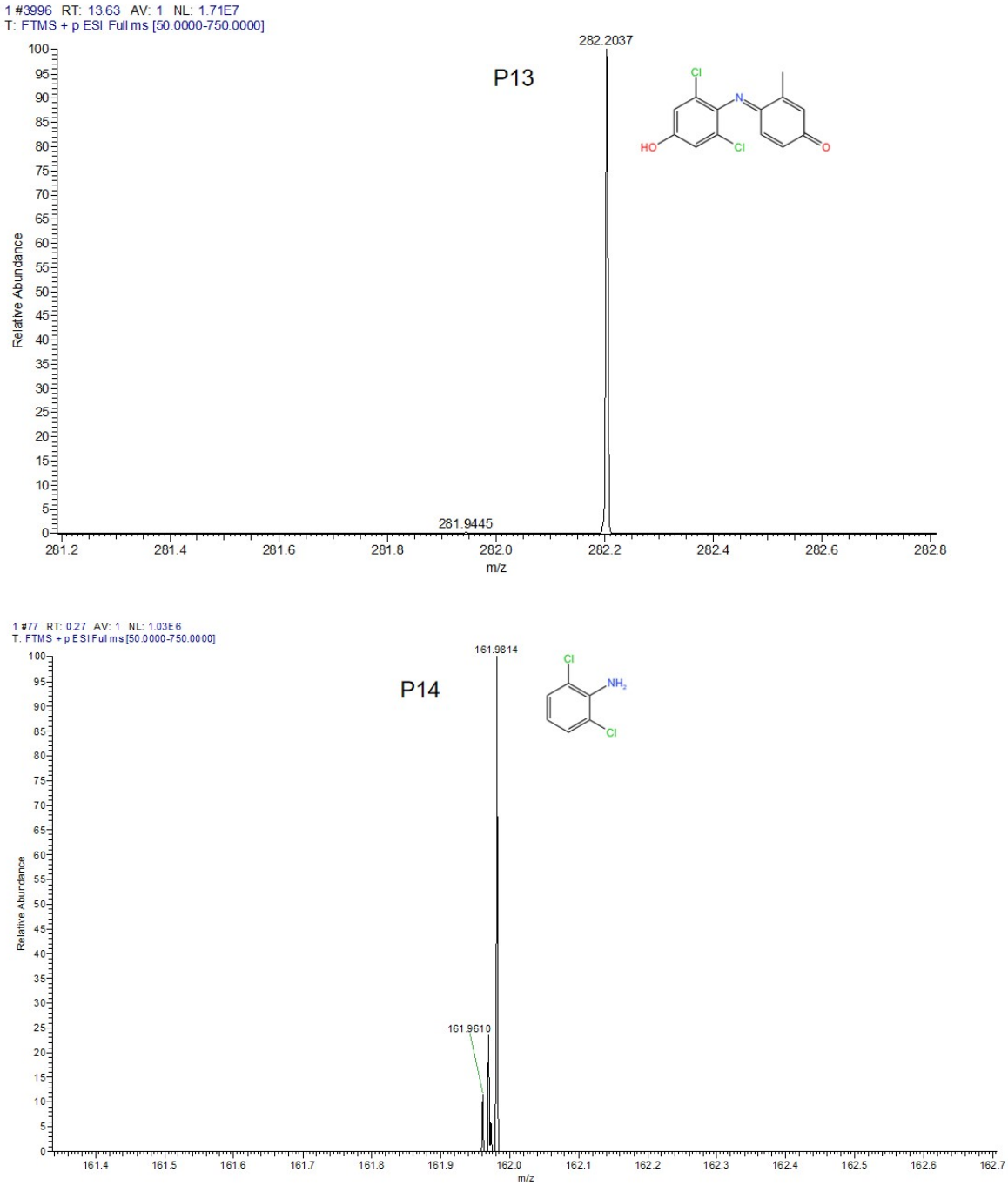

Fig. S10 Liquid chromatogram of DCF intermediate.

References

1. A. Ahmed, A. Hezam, J. Rabeah, C. Kreyenschulte, N. Steinfeldt, S. Wohlrab and J. Strunk, $Bi_2O_{2.33}/Bi_4O_5I_2$-heterojunction photocatalysts for adsorption and visible light-driven degradation of pharmaceutical pollutants, *Catalysis Today*, 2024, 445, 115093.
2. X. Zhang, W. Li, Y. Lei, J. He, Y. Huang and W. Tan, Biomass C-doped three-dimensional Bi_2WO_6 for enhanced visible-light-driven photodegradation of diclofenac and rhodamine B, *Ceramics International*, 2024, 50, 18594-18608.
3. M. Aldrdery, M. Aadil, S. R. Ejaz, A. Khalid, F. Alresheedi, H. D. Alkhaldi, M. I. Saleem, A. E. Jery and M. R. Alrahili, Synergistic role of indium doping and g-C_3N_4 reinforcement in boosting the visible light-triggered rhodamine B and diclofenac sodium salt degradation over rare earth molybdate, *Surfaces and Interfaces*, 2024, 54, 105232.
4. J. Nieto-Sandoval, A. Torres-Pinto, M. Pedrosa, M. Munoz, Z. M. de Pedro, C. G. Silva, J. L. Faria, J. A. Casas and A. M. T. Silva, Application of g-C_3N_4-PVDF membrane for the photocatalytic degradation of micropollutants in continuous flow mode: Impact of water matrix, *Journal of Environmental Chemical Engineering*, 2023, 11, 110586.
5. L. Heon, P. Jaegu, L. Su Shiung, P. Young-Kwon, K. Sang-Chai and J. Sang-Chul, Diclofenac degradation properties of a La-doped visible light-responsive TiO_2 photocatalyst, *Sustainable Chemistry and Pharmacy*, 2021, 25, 100564.
6. C. Sanchez Tobon, I. Panžić, A. Bafti, G. Matijašić, D. Ljubas and L. Ćurković, Rapid Microwave-Assisted Synthesis of N/TiO_2/rGO Nanoparticles for the Photocatalytic Degradation of Pharmaceuticals, *Nanomaterials*, 2022, 12, 3975.
7. W. Zhang, L. Zhou and H. Deng, Ag modified g-C_3N_4 composites with enhanced visible-light photocatalytic activity for diclofenac degradation, *Journal of Molecular Catalysis A: Chemical*, 2016, 423, 270-276.
8. L. Das, S. K. Barodia, S. Sengupta and J. K. Basu, Aqueous degradation kinetics of pharmaceutical drug diclofenac by photocatalysis using nanostructured titania–zirconia composite catalyst, *International Journal of Environmental Science and Technology*, 2014, 12, 317–326.
9. I. A. Garbusova, V. T. Alexanjan, L. A. Leites, I. R. Golding and A. M. Sladkov,

Vibrational spectra of phenylethynylcopper(I), *Journal of Organometallic Chemistry*, 1973, 54, 341-344.

10. G.-Y. Zhao, H.-Y. Li, Y. Yang, Q.-H. Zhao, T.-T. Su and J.-L. Ma, Facile one-step synthesis of PhC_2Cu nanowires with enhanced photocatalytic performance, *Environmental Science and Pollution Research*, 2022, 29, 89681–89690.